

Role of hexamethylenetetramine concentration on structural, morphological, optical and electrical properties of hydrothermally grown zinc oxide nanorods

Guru Nisha Narayanan¹ · Karthikeyan Annamalai¹

Received: 3 May 2016 / Accepted: 14 July 2016 / Published online: 21 July 2016
© Springer Science+Business Media New York 2016

Abstract Zinc oxide (ZnO) nanorods were grown on the glass substrates using hydrothermal method. Influence of hexamethylenetetramine (HMTA) concentration on the morphological, structural, optical and electrical properties of ZnO was investigated. Increasing HMTA concentration produces dense growth of nanorods and decreases the diameter from ~ 450 to ~ 150 nm and also modified the hexagonal shape of ZnO nanorods to circular shape. X-ray diffraction spectra revealed that the synthesized ZnO nanorod exhibits wurtzite structure. Shifting of absorbance edge from 3.30 to 3.36 eV with increasing concentration of HMTA was observed in the UV–Vis spectra. Photoluminescence studies showed the presence of defect related peaks such as zinc interstitial and oxygen vacancies. The observed blue shift in UV emission peak from 387 to 361 nm in photoluminescence spectrum also confirmed the decrease in the size of nanorods. Electrical studies showed the increase in the resistance with the increase in the HMTA concentration from 1.17 to 16.9 k Ω due to dense and reduced size of nanorod networks.

1 Introduction

Zinc Oxide (ZnO), one of the II–VI metal oxide semiconductors, has been widely investigated as it possesses wide direct band gap of 3.37 eV and large exciton binding energy of 60 meV at room temperature [1] and its potential

applications in light emitting diodes [2], field emission devices [3], solar cells [4, 5], super capacitors [6, 7], photocatalysis [8, 9] and gas sensors [10, 11]. Preparation of ZnO nanostructures were reported by pulsed laser deposition [12], rf sputtering [13], spray pyrolysis [14], chemical vapor deposition techniques [15] and also through chemical routes [16]. ZnO nanostructures such as nanowires (NW) [17], nanorods (NR) [18], nanofibers [19], nanotubes (NT) [20], nanoplates (NP) [21], and nanoparticles [22] have been successfully developed employing these techniques. Among these techniques, hydrothermal approach is a promising one for growing ZnO nanorods due to controlled growth rate, simplicity [23] and its ability to produce various nanostructures [24, 25]. High reaction rate in the hydrothermal synthesis process leads to yield structures of different sizes and irregular morphology. Hence, it is necessary to control the reaction process using suitable additives such as organic ligands and surfactants [26] for various applications. A variety of amine molecules such as hexylamine, ethylenediamine, trimethylamine and butylamine were used to synthesize ZnO nanostructures [27, 28].

In this report, ZnO nanorods were synthesized using ZnO seed layer prepared on the micro slide glass substrates using isopropyl alcohol (IPA) based precursor solution and studied the role of various hexamethylenetetramine (HMTA) concentrations on the structural, optical, morphological and electrical properties of ZnO nanorods.

2 Experimental

2.1 Materials

Zinc acetate dihydrate ($\text{Zn}(\text{CH}_3\text{COOH})_2 \cdot 2\text{H}_2\text{O}$, Merck, purity 99.9 %), zinc nitrate hexahydrate (ZNH)

✉ Karthikeyan Annamalai
karthikeyan.a@ktr.srmuniv.ac.in

¹ Department of Physics and Nanotechnology, Centre for Materials Science and Nano Devices, SRM University, Kattankulathur, Kanchipuram, Tamil Nadu 603203, India

($\text{Zn}(\text{NO}_3)_2 \cdot 6\text{H}_2\text{O}$, Sigma-Aldrich, purity 99.9 %), IPA, monoethanolamine (MEA) ($\text{HOCH}_2\text{CH}_2\text{NH}_2$, Merck, purity 99.9 %) and HMTA ($\text{C}_6\text{H}_{12}\text{N}_4$, Sigma-Aldrich, purity 99.9 %) were procured and double distilled water was used. All the reagents procured were of analytical grade and hence used without further purification.

2.2 Synthesis of ZnO nanorods

ZnO nanorods were formed by immersing the ZnO seed layers coated on the well cleaned glass substrates by spin coating technique. The seed layer solution was prepared by a simple sol gel technique as given elsewhere [29]. The ZnO seed layer coated on glass substrate was immersed vertically in aqueous growth solution (containing ZNH (1.4 g) and various concentrations of HMTA (0.1 to 0.5 M) in 50 ml double distilled water) taken in the Teflon-lined autoclave maintained at 90 °C for 3 h. The obtained ZnO nanorods samples were thoroughly washed with distilled water and then annealed at 550 °C for 1 h in air. Annealed ZnO nanorods samples prepared from 0.1, 0.2, 0.3, 0.4 and 0.5 M HMTA concentrations are named as S1, S2, S3, S4 and S5 respectively.

2.3 Characterization techniques

The morphology of ZnO nanorod was examined with field emission scanning electron microscope (FESEM) attached with energy-dispersive X-ray spectroscopic (EDS) analysis using FEI quanta FEG 200. Transmission electron microscopic (TEM) images were recorded using a JEOL JEM 2100F at an accelerating voltage of 200 kV by suspending

the sample in ethanol. Structure of the film was analyzed by PAN analytical X'Pert Pro diffractometer employing $\text{CuK}\alpha$ radiation ($\lambda = 1.5406 \text{ \AA}$) in the 2θ range of 20°–80°. A He–Cd laser of wavelength 325 nm was used as excitation source to study photoluminescence (PL) property of the samples using JASCO spectrofluorometer FP-8600. Optical absorption measurements were carried out using SHIMADZU UV–Vis-spectrophotometer. I–V measurements were performed using Electrochemical Impedance Spectrometer SP-3000.

3 Results and discussion

3.1 Structural analysis

X-ray diffraction (XRD) pattern of ZnO seed layer and ZnO nanorods prepared from different HMTA concentrations are presented in Fig. 1. The observed peak at (2θ) 31.53°, 34.17°, 36.08°, 47.08°, 56.17°, 62.47° and 72.29° corresponds to (1 0 0), (0 0 2), (1 0 1), (1 0 2), (1 1 0), (1 0 3) and (0 0 4) planes respectively (JCPDS Card No. 36-1451) which confirm the formation of hexagonal wurtzite ZnO film on the ZnO seed. The crystalline size of ZnO seed layer was estimated by Debye–Scherrer formula [30] $D = \frac{0.9\lambda}{\beta \cos \theta}$, where D is the crystallite size, λ is the wavelength of X-rays ($\lambda = 1.5406 \text{ \AA}$), θ is the Bragg diffraction angle in degree, and β is the full width half maximum (FWHM) of the XRD peak in radians. The value of D obtained is about 23.7 nm. The sharp diffraction peak at (0 0 2) plane at (2θ) 34.42° (JCPDS: 36-1451) indicates that the ZnO nanorods show preferential growth along c-axis for samples S1–S3

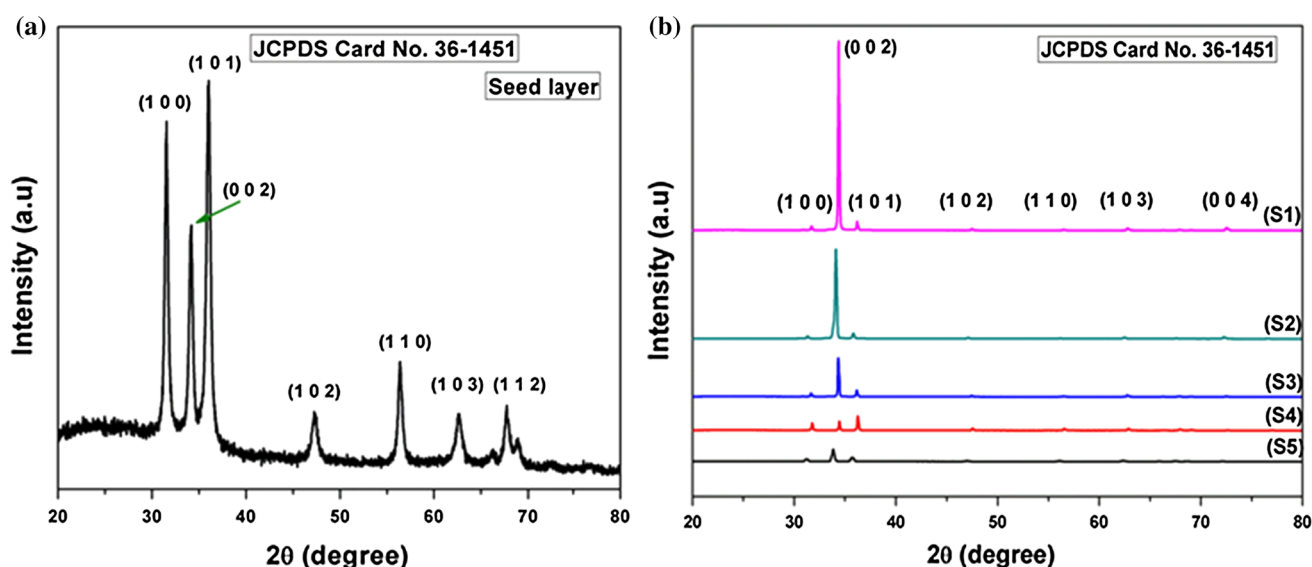


Fig. 1 XRD pattern of **a** ZnO seed layer and **b** synthesized ZnO nanorods thin films

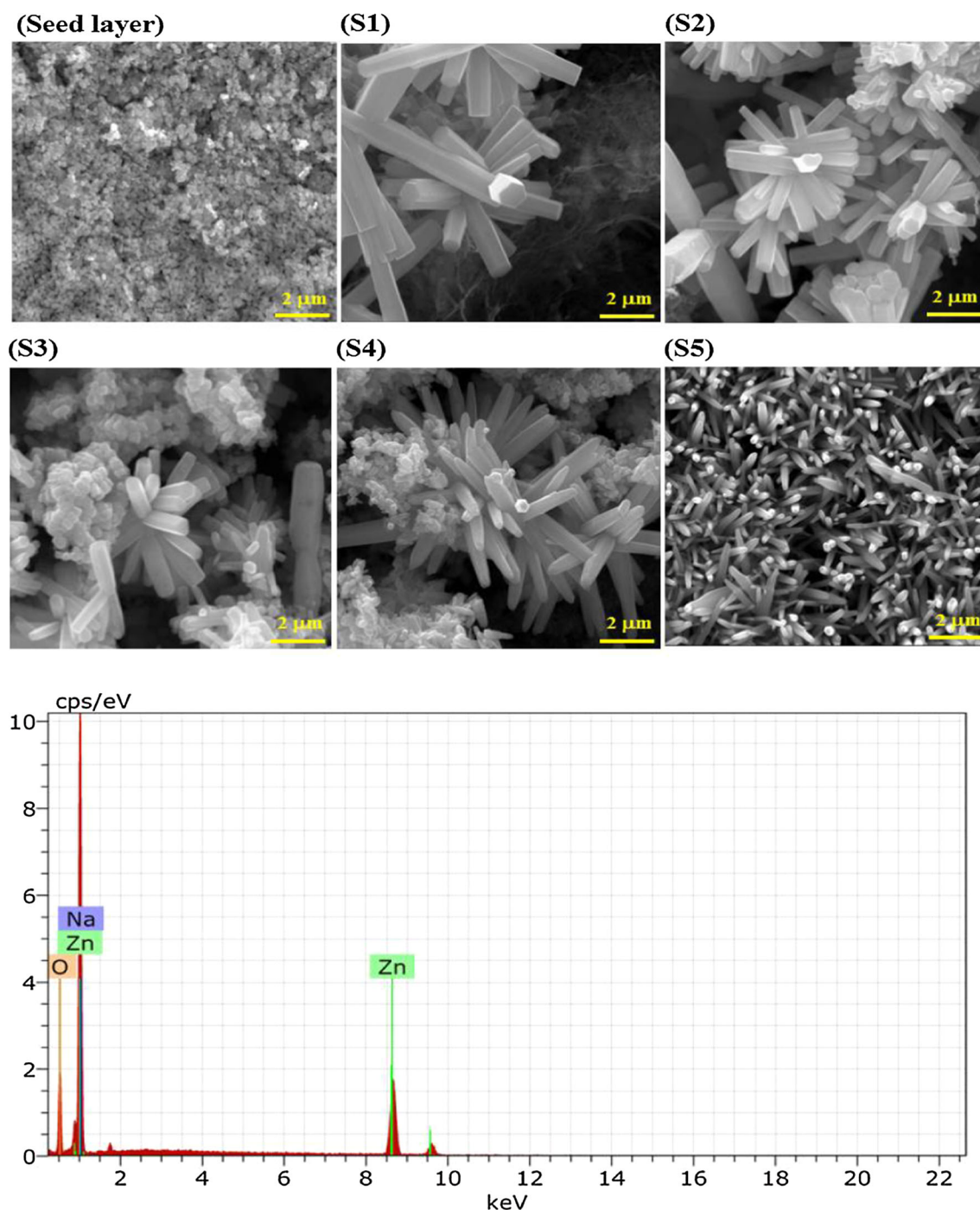


Fig. 2 Surface morphology of ZnO seed layer and ZnO nanorods (S1–S5) with different HMTA concentrations and EDS analysis of the sample S1

(Fig. 1b). As the concentration of HMTA increases, the intensity of (0 0 2) plane decreases whereas the intensity of (1 0 1) plane slightly increases, thus indicating the vertical as well as misaligned growth (S4 and S5). Also, the (0 0 2) plane exhibits a small shift towards the lower angle, implying the tensile strain on the samples [31, 32]. The cell parameters for S1 were calculated using the relations [33]

$a = \frac{1}{\sqrt{3}} \frac{\lambda}{\sin \theta_{(100)}}$ and $c = \frac{\lambda}{\sin \theta_{(002)}}$, where λ (1.5406 Å) is the wavelength of X-rays and $\theta_{(100)}$ and $\theta_{(002)}$ are the angle of diffraction peak of (1 0 0) and (0 0 2) respectively. The values obtained are $a = 3.273$ Å and $c = 5.243$ Å. The c/a ratio calculated is 1.6034 Å which compares well with the value reported by Qiu et al. [34].

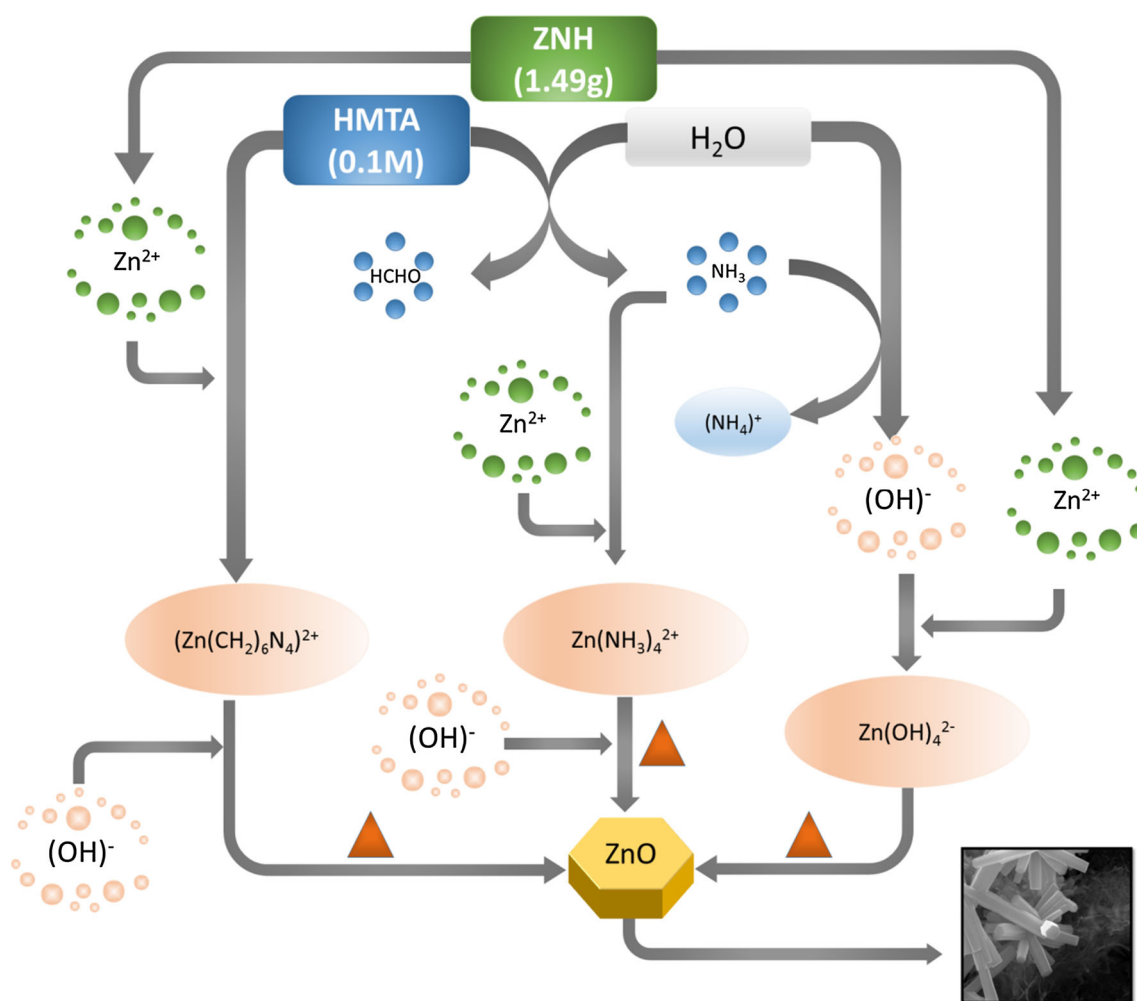


Fig. 3 Schematic illustration of proposed growth mechanism of ZnO nanorods

3.2 Morphological analysis

The surface morphology of the ZnO seed layer and the ZnO nanorods grown on the ZnO seed layer (S1–S5) is presented in Fig. 2. The diameter of the nanorods is decreased from ~450 to ~150 nm with increase in the concentration of HMTA added in the growth process which has effectively modified the shape of the nanorods from hexagonal to circular. Thus, it is evident that the structure of ZnO nanorods can be modified by tuning the concentration of HMTA. EDS spectrum of sample S1 shows the presence of Zn, O and Na elements. The source for the observed Na is due to the migrated Na from the glass substrate during process of annealing at 550 °C [29].

According to Baruah and Dutta [35], HMTA can attach to nonpolar ZnO crystals surface by a dative covalent bond or hydrogen bond. So, at low concentration of HMTA, the dynamic equilibrium between the attached molecules and

those in the solution exists in such a way that the amounts of HMTA molecules adsorbing onto the ZnO nanorods are lesser. This reduces the steric hindrance between HMTA molecules adhering onto the nearby ZnO nanorods resulting in lateral growth of the ZnO nanorods (as shown in Fig. 2a). When the concentration of HMTA increases, the coverage of HMTA over ZnO nanorods is greater resulting in existence of increased steric hindrances between adjacent nanorods, causing the ZnO nanorods to grow in vertically [36].

The mechanism involved in the formation of ZnO nanorods is as follows: (CH₂)₆N₄ breaks up into ammonia (4NH₃) and formaldehyde (HCHO). Ammonia reacts with water to produce OH⁻ ions. Under the appropriate temperature and pH (5–6), Zn²⁺ is considered to exist in Zn(NH₃)₄²⁺ and Zn(OH)₄²⁻. The dehydration of these intermediates results in the formation of ZnO [37, 38]. The schematic illustration of proposed growth mechanism of ZnO nanorods is shown in Fig. 3.

3.3 Microstructure analysis

TEM images recorded for sample S1 using a JEOL JEM 2100F at an accelerating voltage of 200 kV by suspending the sample in ethanol is presented in Fig. 4. These figures evidently show the formation of nanorods of ZnO.

3.4 Optical properties

The room temperature PL spectrum of ZnO nanorods (Fig. 5a) prepared at various concentrations of HMTA shows three peaks. It is generally characterized by near-band-edge (NBE) UV emission and at least one broad band due to deep level emission (DLE) at visible region ranging from 400 to 750 nm. The UV emission is due to the

recombination of free-exciton [39]. The blue-shift observed from 387 nm (S1) to 361 nm (S5) is due to decrease in the diameter of ZnO nanorods. A similar blue-shift in UV emission peak was reported by Yousefi and Kamaluddin [40] and Wang et al. [41] attributed to reduced size. Emission in the visible region (violet peak around 418 nm and red peak around 648 nm) may be due to defects such as oxygen vacancy (V_O), Zinc vacancy (V_{Zn}), oxygen interstitial (O_i), zinc interstitial (Zn_i), oxygen anti-site (O_{Zn}) and zinc anti-site (Zn_O) [39]. The maximum intensity around 418 nm obtained for the sample S4 (prepared by 0.4 M HMTA) as shown in Fig. 5a may be due to increase in defects caused by the misaligned growth of ZnO nanorods leading to poor crystallinity as revealed by the XRD spectra.

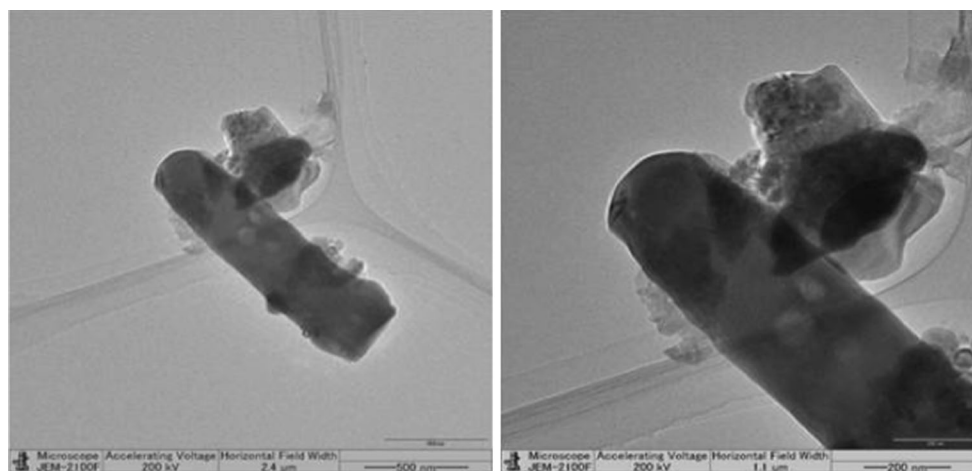


Fig. 4 TEM images for sample S1 at different magnifications

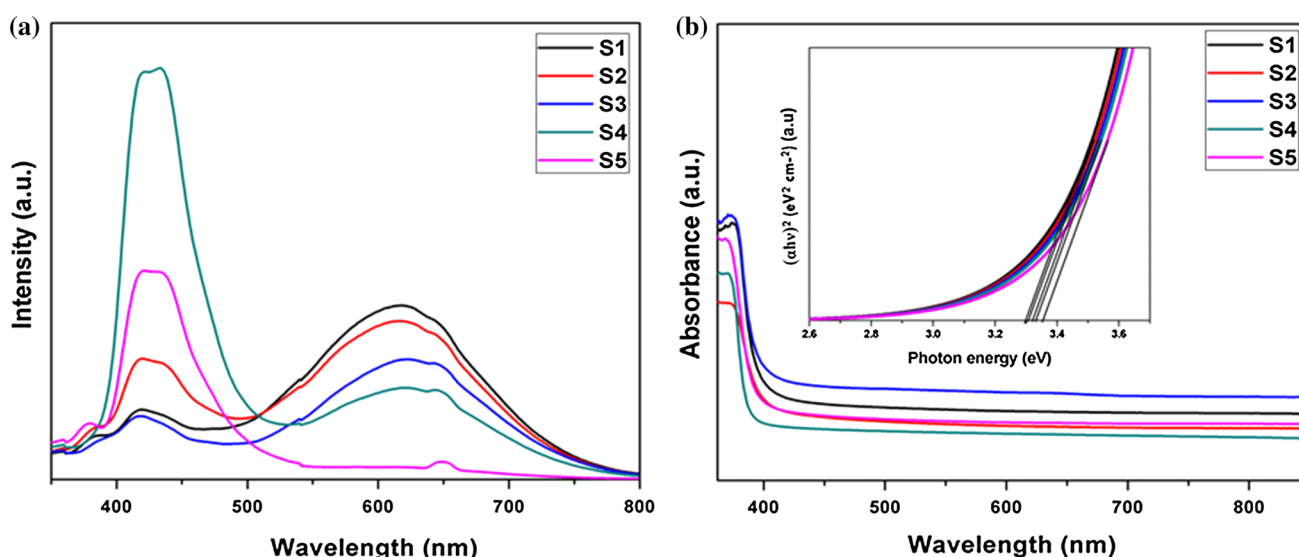


Fig. 5 **a** PL spectra of ZnO nanorods and **b** UV–visible absorbance spectra of ZnO nanorods. The inset shows the Tauc plot for the samples

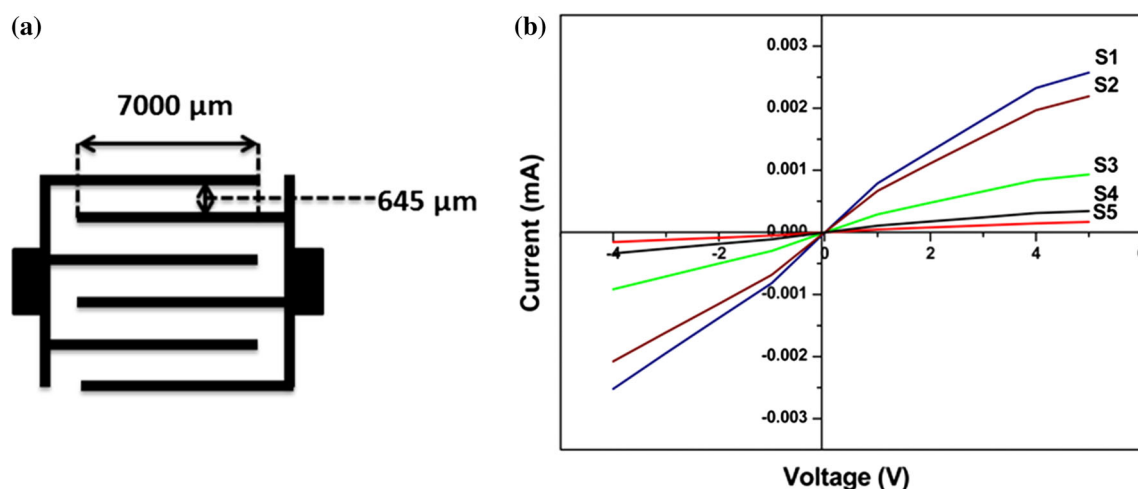


Fig. 6 **a** Schematic illustration of electrodes **b** I–V characteristics of ZnO nanorods prepared from different concentrations of HMTA

Optical bandgap (E_g) of the films was calculated using the relation $(\alpha h\nu) = A(h\nu - E_g)^n$, where $n = 1/2$ for direct bandgap semiconductor, A is a constant, h is the Planck's constant and α is the absorption coefficient [42]. The band gap calculated is 3.30, 3.32, 3.33, 3.34 and 3.36 eV for the samples S1, S2, S3, S4 and S5 respectively (Fig. 5b). Thus it is evident that bandgap increases systematically as the diameter of ZnO nanorods decreases due to the size effect of ZnO nanorods [43].

3.4.1 Electrical properties

I–V characteristics were measured by electrochemical impedance spectrometer SP-3000 instrument using interdigitated gold electrode structure deposited over ZnO nanorods through shadow mask by thermal evaporation technique. Figure 6a shows the schematic representation of the electrodes and the measured I–V characteristics are shown in Fig. 6b. From the resistance calculated at 1 V, it was found that for lower HMTA concentration, the sample (S1) produced resistance of 1.17 k Ω and for higher concentrations of the HMTA, the samples (S2, S3, S4 and S5) showed increased resistance values of 1.44, 3.30, 7.13 and 16.99 k Ω respectively. This confirms that the misaligned growth, reduced diameter and increased density of ZnO nanorods causing increased resistance. As, the contacts across the nanorod networks are dissimilar, the current–voltage curves show non-linear behavior.

4 Conclusion

ZnO nanorods were grown using the hydrothermal method on ZnO seed layer coated glass substrate. Lower concentration of HMTA in the growth solution produces hexagonal shaped nanorods with diameter around 450 nm

showing preferential growth along (0 0 2) plane. Increased HMTA concentration yields circular nanorods with diameter around 150 nm and increased density as revealed by SEM images. At lower HMTA concentration, lateral growth of ZnO nanorods was observed due to less steric hindrance effect between HMTA molecules adhering onto the nearby ZnO nanorods. When the concentration of HMTA increased, the coverage of HMTA over ZnO Nanorods is greater resulting vertical and highly dense growth of nanorods with reduced diameter. PL investigation revealed blue shift in UV emission spectrum and also showed the presence of defect related peaks such as zinc interstitial and oxygen vacancies. UV–Vis spectra showed the systematic change of optical bandgap indicating the size reduction with increased HMTA concentration. I–V Characteristics of these samples showed increase in resistance value from 1.17 to 16.99 k Ω with increased HMTA concentration (from 0.1 to 0.5 M) confirms the change in structural and contact nature of nanorod networks.

Acknowledgments The authors thank SRM University, Kattankulathur, Kanchipuram (Dt.) for the award of SRM fellowship to carry out the research work. The authors are grateful to Prof. K. Ramamurthi for his valuable suggestions during the course of this work. The authors thank Prof. John Thiruvadigal for extending the experimental facilities created under DST–FIST (DST–FIST–SR/FST/PSI-155/2010) and Nanotechnology Research Center, SRM University, Kattankulathur-603 203 for extending the characterization facilities.

References

1. C.C. Chen, N. Ye, C.F. Yu, T. Fan, J. Ceram. Process. Res. **15**, 102–106 (2014)
2. H. Huang, G. Fang, X. Mo, H. Long, L. Yuan, B. Dong, X. Meng, X. Zhao, IEEE Electr. Device Lett. **30**, 1063–1065 (2009)
3. C.X. Xu, X.W. Sun, Appl. Phys. Lett. **83**, 3806–3808 (2003)

4. Q. Zhang, C.S. Dandeneau, X. Zhou, G. Cao, *Adv. Mater.* **21**, 4087–4108 (2009)
5. E. Guillen, L.M. Peter, J.A. Anta, *J. Phys. Chem. C* **115**, 22622–22632 (2011)
6. O. Harnack, C. Pacholski, H. Weller, A. Yasuda, J.M. Wessels, *Nano Lett.* **3**, 1097–1101 (2003)
7. A. Kathalingam, V. Senthilkumar, S. Valanarasu, J.-K. Rhee, *Semicond. Sci. Technol.* **27**, 105006 (2012)
8. Y. Lu, L. Wang, D. Wang, T. Xie, L. Chen, Y. Lin, *Mater. Chem. Phys.* **129**, 281–287 (2011)
9. M. Rezapour, N. Talebian, *Mater. Chem. Phys.* **129**, 249–255 (2011)
10. J. Zhang, S. Wang, M. Xu, Y. Wang, B. Zhu, S. Zhang, W. Huang, S. Wu, *Cryst. Growth Des.* **9**, 3532–3537 (2009)
11. S. Tian, F. Yang, D. Zeng, C. Xie, *J. Phys. Chem. C* **116**, 10586–10591 (2012)
12. D. Valerini, A. Creti, A.P. Caricato, M. Lomascolo, R. Rella, M. Martino, *Sens. Actuators B Chem.* **145**, 167–173 (2010)
13. N.H. Al-Hardan, M.J. Abdullah, A.A. Aziz, *Int. J. Hydrog. Energy* **35**, 4428–4434 (2010)
14. P. Singh, A. Kaushal, D. Kaur, *J. Alloys Compd.* **471**, 11–15 (2009)
15. D. Barreca, D. Bekermann, E. Comini, A. Devi, R.A. Fischer, A. Gasparotto, C. Maccato, G. Sberveglieri, E. Tondello, *Sens. Actuators B Chem.* **149**, 1–7 (2010)
16. C. Wu, X. Qiao, J. Chen, H. Wang, F. Tan, S. Li, *Mater. Lett.* **60**, 1828–1832 (2006)
17. Y. Ding, Y. Liu, K.C. Pradel, Y. Bando, N. Fukata, Z.L. Wang, *Micron* **78**, 67–72 (2015)
18. R. Wahab, Y.-S. Kim, H.-S. Shin, *Curr. Appl. Phys.* **11**, 334–340 (2011)
19. H.-U. Lee, K. Ahn, S.-J. Lee, J.-P. Kim, H.-G. Kim, S.-Y. Jeong, C.-R. Cho, *Appl. Phys. Lett.* **98**, 193114 (2011)
20. C.-Y. Su, A.M. Goforth, M.D. Smith, P.J. Pellechia, H.-C. zur Loye, *J. Am. Chem. Soc.* **126**, 3576–3586 (2004)
21. J. Chang, E. Waclawik, *Cryst. Eng. Commun.* **14**, 4041–4048 (2012)
22. J. Lian, Y. Liang, F.-L. Kwong, Z. Ding, D.H.L. Ng, *Mater. Lett.* **66**, 318–320 (2012)
23. K.G. Yim, M.S. Kim, S. Kim, J.Y. Leem, G. Nam, S.M. Jeon, D.Y. Lee, J.S. Kim, J.I. Lee, *J. Korean Chem. Soc.* **60**, 1605–1610 (2012)
24. Y. Tong, Y. Liu, L. Dong, D. Zhao, J. Zhang, Y. Lu, D. Shen, X. Fan, *J. Phys. Chem. B* **110**, 20263–20267 (2006)
25. C.P. Burke Govey, N.O.V. Plank, *J. Vac. Sci. Technol. B* **31**, 06F101 (2013)
26. M. Navaneethan, J. Archana, M. Arivanandhan, Y. Hayakawa, *Chem. Eng. J.* **213**, 70–77 (2012)
27. M. Navaneethan, K.D. Nisha, S. Ponusamy, C. Muthamizhchelvan, *Mater. Chem. Phys.* **117**, 443–447 (2009)
28. K. Nose, H. Fujita, T. Omata, S. Matsuo, H. Nakamura, H. Maeda, *J. Lumin.* **126**, 21–26 (2007)
29. G.N. Narayanan, R. Ganesh Sankar, A. Karthigeyan, *Thin Solid Films* **598**, 39–45 (2016)
30. M.H. Frey, D.A. Payne, *Phys. Rev. B* **54**, 3158–3168 (1996)
31. H.-W. Chen, H.-W. Yang, H.-M. He, Y.-M. Lee, *J. Phys. D. Appl. Phys.* **49**, 025306 (2016)
32. Q. Yang, H. Cai, Z. Hu, Z. Duan, X. Yang, J. Sun, N. Xu, J. Wu, *Nanoscale Res. Lett.* **9**, 31 (2014)
33. M. Tiemann, F. Marlow, J. Hartikainen, O. Weiss, M. Linder, *J. Phys. Chem. C* **112**, 1463–1467 (2008)
34. J. Qiu, X. Li, W. He, S.-J. Park, H.-K. Kim, Y.-H. Hwang, J.-H. Lee, Yang-Do Kim, *Nanotechnology* **20**, 155603 (2009)
35. S. Baruah, J. Dutta, *Sci. Technol. Adv. Mater.* **10**, 013001 (2009)
36. V. Strano, R.G. Urso, M. Scuderi, K.O. Iwu, F. Simone, E. Ciliberto, C. Spinella, S. Mirabella, *J. Phys. Chem. C* **118**, 28189–28195 (2014)
37. R. Wahab, Y.-S. Kim, K. Lee, H.-S. Shin, *J. Mater. Sci.* **45**, 2967–2973 (2010)
38. S. Guillemin, L. Rapenne, H. Roussel, E. Sarigiannidou, G. Bremond, V. Consonni, *J. Phys. Chem. C* **117**, 20738–20745 (2013)
39. M. Willander, O. Nur, J.R. Sadaf, M.I. Qadir, S. Zaman, A. Zainelabdin, N. Bano, I. Hussain, *Materials* **3**, 2643–2667 (2010)
40. R. Yousefi, B. Kamaluddin, *J. Alloys Compd.* **479**, 11–14 (2009)
41. X.D. Wang, Y. Ding, C.J. Summers, Z.L. Wang, *J. Phys. Chem. B* **108**, 8773–8777 (2004)
42. B.D. Viezbicke, S. Patel, B.E. Davis, D.P. Birnie III, *Phys. Status Solidi B* **252**, 1700–1710 (2015)
43. X. Zhang, J. Qin, Y. Xue, P. Yu, B. Zhang, L. Wang, R. Liu, *Sci. Rep.* **4**, 4596–4604 (2014)